Available online at www.sciencedirect.com
SCIENCE DIRECT
Earth and Planetary Science Letters 246 (2006) 207–216
EPSL
www.elsevier.com/locate/epsl

Periodic slow earthquakes on the flank of Kīlauea volcano, Hawai'i

Benjamin A. Brooks [a,*], James H. Foster [a], Michael Bevis [b], L. Neil Frazer [a], Cecily J. Wolfe [a], Mark Behn [c]

[a] School of Ocean and Earth Science and Technology, University of Hawai'i, 1680 East–West Rd, Honolulu, HI 96816, USA
[b] Geodetic Science, Ohio State University, 2036 Neil Ave. Mall, Columbus, OH 43210, USA
[c] Department of Geology and Geophysics, Woods Hole Oceanographic Institution, Woods Hole, MA 02543, USA

Received 21 December 2005; received in revised form 16 March 2006; accepted 20 March 2006
Available online 22 May 2006
Editor: S. King

Abstract

We analyze 8 years of continuous GPS data from the Hilina slump (HS) on Kīlauea volcano's south flank and identify 3 new slow earthquake (SE) events. The new SEs are very similar to the previously identified one from November 2000, suggesting they share a common source. The series of SEs are separated by regular periods of 774 (±7) days. None of the newly identified events are associated with increased rainfall rates, precluding rainfall as a necessary SE trigger. All of the SEs are followed by increased microseismicity in a ~NW–SE trending band in the southern HS, suggesting that the SEs trigger seismicity. SE location and source parameters are not well-constrained by the CGPS network, although moment can be constrained adequately for the January 2005 event. Using this as a reference, we calculate for the four events equivalent moment magnitude values of 5.6, 5.7, 5.5, and 5.8, in their order of occurrence.

Keywords: slow earthquakes; deformation; GPS geodesy; landslide; tsunami

1. Introduction

Following the initial detection of 'silent' or slow earthquakes (SE) using strainmeters [1–3], continuous GPS (CGPS) observations have led to the discovery of silent after-slip events after conventional subduction zone earthquakes in Japan [4], a SE in the Cascadia Subduction Zone unassociated with a conventional earthquake [5], and recognition that Cascadia SEs are periodic [6] and accompanied by seismic tremor [7]. The first SE detected in an intraplate setting occurred in November 2000 following intense rainfall at the Hilina slump (HS) on Kīlauea volcano's south flank [8]. Because of their increasingly widespread detection [9–12] much recent work has focused on developing a mechanical explanation for subduction zone SEs. Some workers have argued that the tremor associated with the episodic slip (now termed ETS – 'Episodic Tremor and Slip') is closely related to 'harmonic tremor', a seismic phenomenon frequently observed in the early stages of an eruption and which is thought to be driven by forced fluid flow [13]. It has been suggested that ETS is driven by water released during metamorphic phase changes at the interface between a subducting and overriding plate [14–16].

It is unclear, however, whether ETS is applicable in other types of actively deforming regions where

* Corresponding author.
E-mail address: bbrooks@soest.hawaii.edu (B.A. Brooks).

0012-821X/$ - see front matter © 2006 Elsevier B.V. All rights reserved.
doi:10.1016/j.epsl.2006.03.035

SEs have occurred, such as strike–slip plate boundaries [1] or volcano flanks [8], where there are distinctly different rheological conditions. At Kīlauea's Hilina slump (HS), for instance, because the event followed a period of intense rainfall, Cervelli et al. [8] suggested a SE-triggering mechanism where percolating rainwater acted to lubricate a slip plane at ~5 km depth.

In this study, we identify 3 new Hilina slump SEs that are very similar to the November 2000 SE, suggesting they share a common source. We find that none of the new events are associated with significant rainfall and that they consistently trigger microearthquakes in a specific location within the HS. More surprisingly, we find that the series of 4 SEs is apparently periodic: 774-day (±7-day) intervals separate each event. As rainfall is clearly not a necessary condition for SEs to occur, and as the SEs likely occurred in a well-hydrated wedge shallower than ~10 km, our results suggest that if a general theory is to be developed to explain SE occurrence and periodicity, it should consider a wider range of mechanical conditions than previously thought.

2. Kīlauea's mobile south flank

The Hawaiian Volcano Observatory (HVO), the University of Hawai'i, and Stanford University jointly operate a network of continuous GPS (CGPS) stations focused on Kīlauea volcano (Fig. 1). Data from the CGPS network and periodically reoccupied survey GPS sites demonstrate that under the influence of some combination of gravitational and magmatic forces, Kīlauea's entire south flank, known as the 'Hilina slump' (HS), currently slides seaward at average rates of ~6–10 cm/yr [17,18] (Fig. 1B). Underlain by a gently north-dipping decollement at depths of ~7–11 km, fully 3/4 of the HS is expressed offshore as a submarine landslide [19–21] that poses a major tsunami hazard both locally and across the eastern Pacific basin [22,23]. Microseismicity in the region is dominated by decollement events [24] and the decollement has been postulated as the source for large recent earthquakes such as the 1975 *M* 7.2 Kalapana [25] and 1868 *M* 7.7 Great Ka'ū earthquakes [26,27].

It is generally believed that Kīlauea's southwest and east rift zones (SWRZ, ERZ) delineate the HS's upslope boundary (e.g. 28]) and that the ~500 m high, south-facing scarps of the Hilina Pali represent normal faults in the headwall of the HS. The downdip continuity of the Hilina Pali fault plane has been debated with some authors suggesting the faults continue to depth and intersect the decollement [29] while others suggest the faults shoal at shallow depths [30,31]. The different geometric scenarios have distinctly different implications for HS wedge kinematics and tsunamigenesis: slip occurring on a shoaling Hilina Pali fault would not be expected to induce as much slip on the decollement as a Hilina Pali fault which extended to greater depths. The latter scenario might be expected to generate larger submarine volume movements and associated tsunamis than the former.

3. GPS processing and displacement estimates

Our analysis of the CGPS data from the Kīlauea network comprises estimating both long term velocities over yearly time-scales and the magnitude of discrete displacements occurring over periods of days. To estimate long-term velocities we perform daily regional geodetic analyses on CGPS measurements from all available Hawai'i stations and fiducial sites around the Pacific using the GAMIT and GLOBK software [32] and precise orbits computed by the Scripps Orbit and Permanent Array Center (SOPAC) (http://sopac.ucsd.edu). For more details on our long-term velocity determination we refer the reader to Caccamise et al. [33].

We estimate the magnitude of discrete displacements using a robust least squares fit to a step function and a linear velocity for each component. A window of 20 days either side of the event is used for the fit. This was empirically determined to optimize the trade-off between minimizing the impact of short period (3–7 days) correlated "noise" in the time series that might bias the step estimates and real, longer period changes in the velocities that would require more parameters to estimate. The formal errors for this fit represent the uncertainties in the displacement estimates.

In a Pacific plate-fixed reference frame, the time series solutions show the HS CGPS sites moving seaward at an average rate of ~6–10 cm/yr, punctuated by discrete steps of millimetres to a few centimetres displacement over periods of a few days (Fig. 2). It is important to note that these data are well-suited for event detection because hydrological loading effects do not complicate the GPS displacement records as they do in many continental settings [34].

In Figs. 2A and 3, we identify a total of 3 new discrete SE events along with the November 2000 event [8] and a major dyke intrusion from Kīlauea's east rift zone [35]. The displacements associated with the SEs are clearly significant at the 95% confidence level (Figs. 1 and 3) and they stand out from other transient motions in the time series because of their similar location and

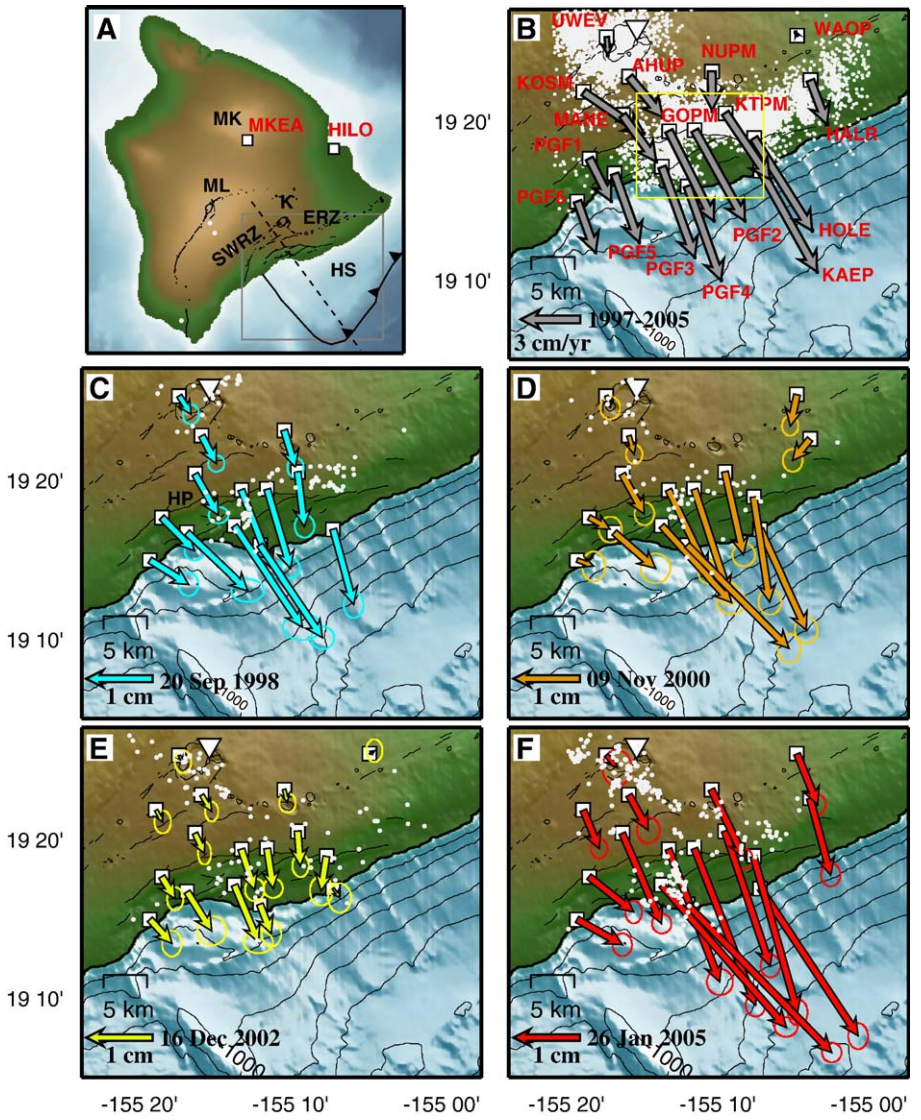

Fig. 1. Continuous GPS data from Kīlauea network. (A) Location map with study area shown by grey box. ML, Mauna Loa volcano; MK, Mauna Kea volcano; K, Kīlauea volcano; HS, Hilina slump. SWRZ and ERZ are northward limits of the HS-bounding south-west and east Kīlauea rift zones. White boxes are GPS stations shown in panels C–F, and in Figs. 2 and 3. Dashed line is the location of the cross-section shown in Fig. 5. (B) Average yearly velocities (grey arrows) from GPS stations (red text) for 1997–2005, ellipses indicate 2σ errors. White dots are seismicity from the HVO catalog archived at the Northern California Earthquake Data Center for the same time period. Only those earthquakes occurring in the HS volume and at depths less than 20 km are shown. Yellow box is the area from which seismicity analyzed in Fig. 3 is sampled. Inverted white triangle is the rain gauge site at National Park service headquarters. (C) HP indicates the position of the Hilina Pali scarp. (C–F) Slow earthquake displacements for 20 Sept., 1998 (C); 9 Nov. 2000 (D); 16 Dec. 2002 (E); and 26 Jan. 2005 (F). Only seismicity from ±10 days is shown.

spatially coherent displacement patterns expected from repeated slow slip events on the same buried surface. Most of the motion at each site occurs within the first 24–48 h of event onset, but some sites show some residual motion up to ~5 days (Fig. 3). The four events are separated by intervals of ~25.5 months (781, 767, and 772 days, respectively) and none are accompanied by earthquakes greater than M 3.5 (see Section 5).

The relative surface displacements during the December 2002 event are 2–3 times smaller than those during the next largest event and as much as an order of magnitude smaller at sites PGF4 and KAEP (Fig. 1E); nonetheless, its existence is well supported by the rest of the GPS data (Fig. 3C). The SEs appear to be periodic. Even if we ignore the 2002 event, then the time intervals (Nov. 2000 – Jan. 2005) and (Sept.

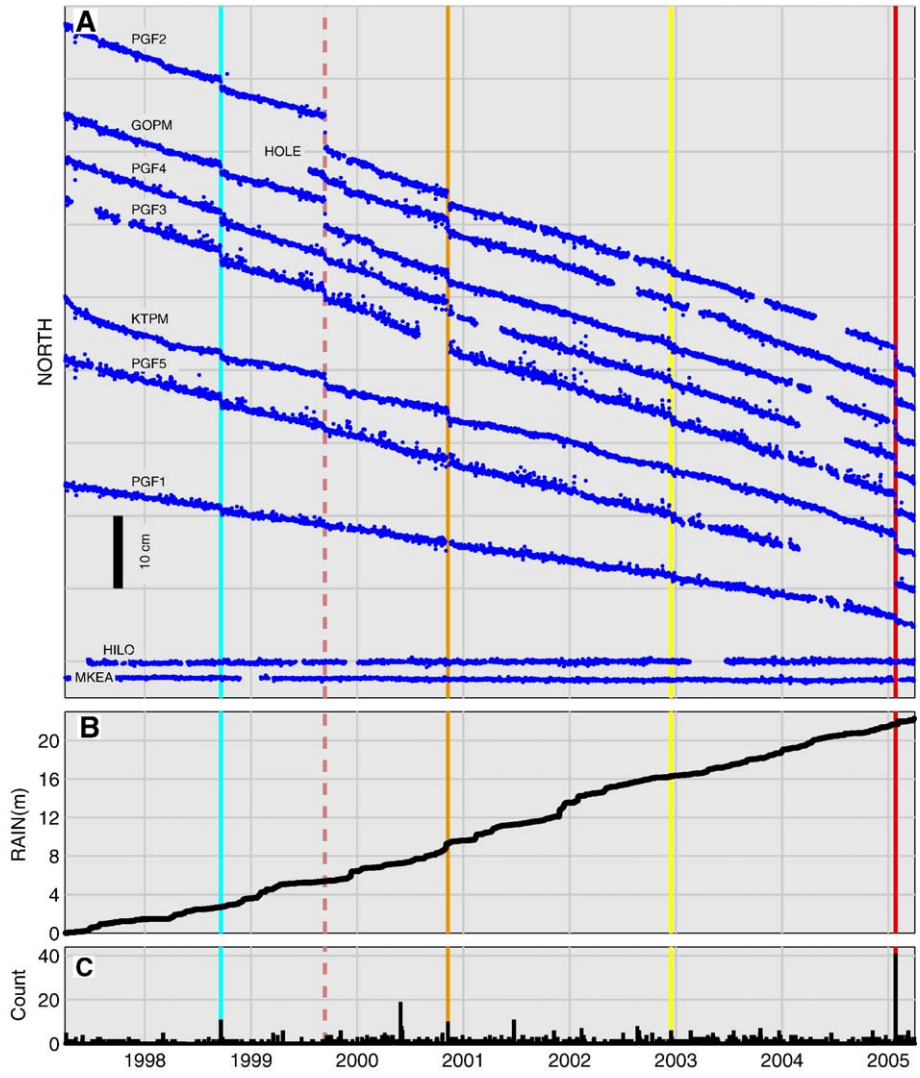

Fig. 2. (A) Daily solution time series of relative northward motion of GPS stations indicated in Fig. 1. Stations HILO and MKEA shown as stable references. Four slow earthquakes colored as in Fig. 1. Dashed pink line indicates September 1999 dyke intrusion. Vertical dashed red line indicates the time of the event. (B) Cumulative rainfall measured at the National Park Service headquarters (see Fig. 1 for location). (C) Daily counts of earthquakes within the slump volume (19°21′55″:19°33′43″N, −155°31′10″:−155°14′62″W, 0.20 km depth) from the HVO catalog archived at the Northern California Earthquake Data Center.

1998 – Nov. 2000) have durations in the ratio 1.97:1, which differs only by 1.5% from the integer ratio 2:1. Once the 2002 event is included, all three intervals have a similar duration falling in the range 774± 7 days. While interseismic strain rates near a locked subduction zone (as in Cascadia) are expected to vary very little from one year to the next, the temporal development of strain in the near-field of an actively erupting volcano is expected to be less steady due to temporal variation in the stress field [36]. Even for Cascadia SE events, some GPS stations do not record all of the jumps observed at other stations. It is not unreasonable that event amplitudes would be rather more heterogeneous at Kīlauea.

Fig. 2B shows cumulative rainfall since 1998 for a site near Kīlauea caldera and demonstrates that, although there certainly was a large rainfall event (>1 m) a week prior to the November 2000 SE, no such relationship exists with the other SEs. Moreover, large rainfall events elsewhere in the time series are not accompanied with obvious deformation events and we conclude that heavy rainfall is not a necessary condition for a slow earthquake to occur at the HS. This does not, however, preclude the possibility that cumulative

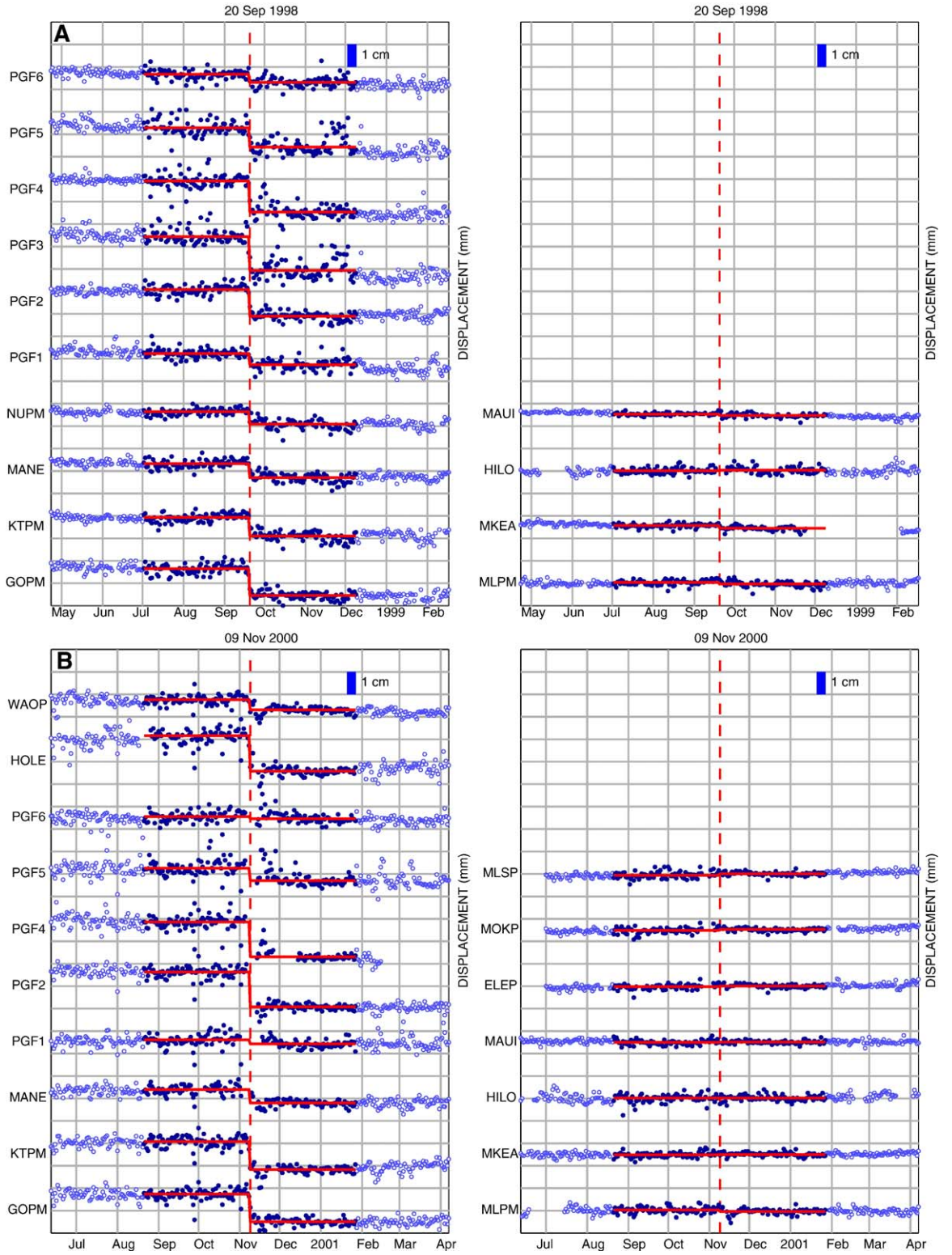

Fig. 3. Detrended time series for the North component of stations indicated in Fig. 1B for each of the four SE events. Solid blue dots, indicates a window of 80 days either side of the event. Red line indicates the fit to a step function and a linear velocity: (A) 20 Sept., 1998; (B) 9 Nov. 2000; (C) 16 Dec. 2002; (D) 26 Jan. 2005.

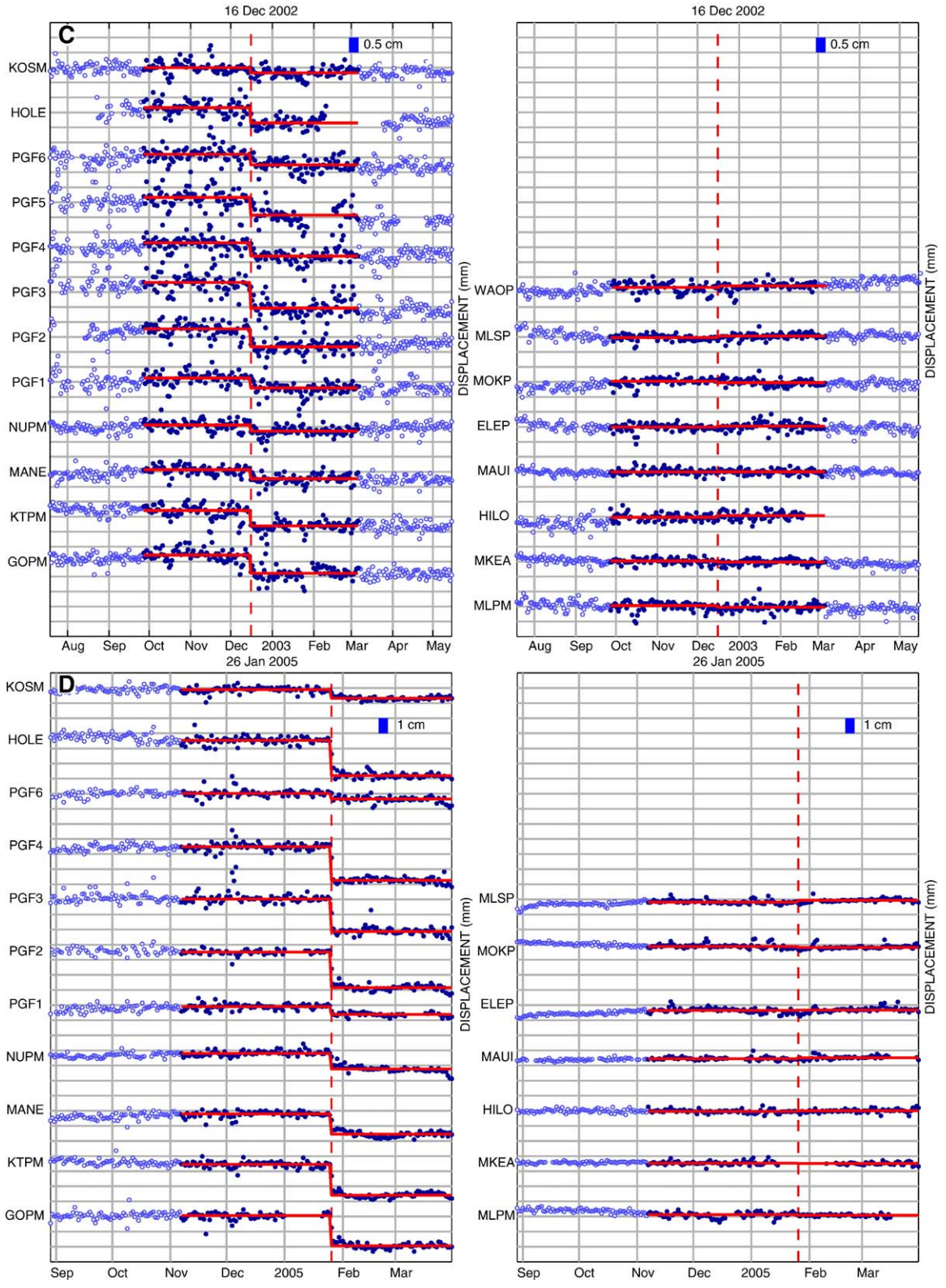

Fig. 3 (*continued*).

rainwater filtration to seismogenic depths may still exert some influence on deformational activity.

4. Inversion for slow earthquake source parameters

In order to investigate SE source mechanism we follow Brooks and Frazer [38] and use a Monte Carlo-based Gibbs sampling (GS) algorithm to invert surface displacements for the 9 non-linear parameters describing the geometry and kinematics of a rectangular dislocation in an elastic half-space [37]. Our goal is not simply to obtain an optimal solution, but rather to estimate posterior densities for their value as indicators of resolution and uncertainty. This is especially important for two reasons: first, sampling geometry is spatially biased because the CGPS network is restricted by the shoreline and simply reporting an optimal model may seriously misrepresent the complexity of parameter/misfit space; second, the HS is a potential tsunami hazard both locally and for the Pacific region and mischaracterization of uncertainties associated with its behaviour is very undesirable.

In Fig. 4A–C we present the inversion results for the January 2005 event as marginal posterior probability distributions; results for each of the other events are similar. To help constrain the inversion, we limit the strike range of possible solutions to ±30° from east–west. A well-constrained solution would be reflected in strongly peaked distributions for each parameter (i.e. Fig. 4C, Brooks and Frazer [38]). For the HS events, however, the lack of strong modality reflects a poorly constrained problem. This is not to say that models that mimic the data extremely well cannot be found; rather, the inversion finds too many equivalently good ones. A wide family of geologically plausible models, ranging from shallow thrust faults at depths of ~3–5 km similar to that of Cervelli et al. [35] to deeper seated normal faults shoaling into the basal decollement at ~6–8 km depth, fit the data to better than ~5–7 mm in an RMS sense (Fig. 5).

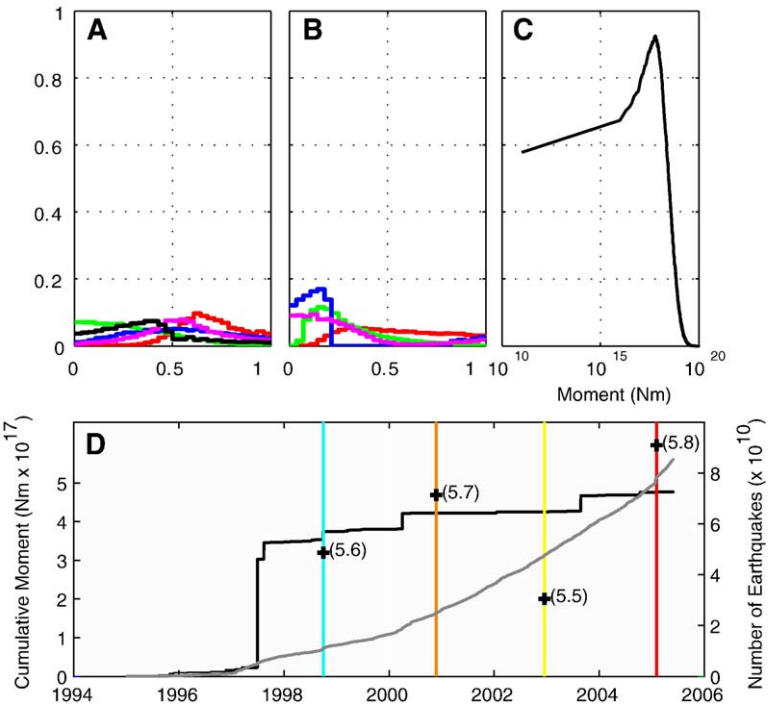

Fig. 4. Marginal posterior probability distributions from Gibbs Sampling inversion of the January 2005 event. Distributions from other SEs are nearly identical. (A) Location of dislocation upper left corner: longitude (red, −155°22′37.2″:−155°2′45.96″); latitude (green, 19°9′28.4′:19°17′50.64″ N); depth (blue, 0:20 km). Fault slip: strike–slip (magenta, −5:5 m); dip–slip (black, −5:5 m). (B) Fault geometry: length (red, 0:40 km); width (green, 0:40 km). Fault orientation: strike (blue, 60:120°, 240:300°); dip (magenta, 0:90°). To help constrain the inversion, we limit the strike range to ±30 degrees from east–west. (C) For the January 2005 SE, marginal distribution for moment defined as the product of dislocation length, width, slip and shear modulus, here taken to be 3×10^{10} GPa. (D) Seismic moment, M_0 (crosses) and equivalent moment magnitude, M_w (value in parentheses) for the SEs calculated using the peak value from panel C. Black line, cumulative earthquake moment from the HS volume. Data source as in Fig. 1. Gray line, cumulative number of earthquakes in HS volume. Colored lines, SE events as in Fig. 1.

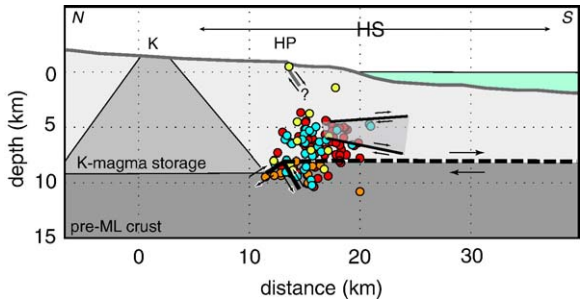

Fig. 5. Cross-section of Kīlauea's south flank along dashed line in Fig. 1 after Got and Okubo [24]. K, Kīlauea. HP, Hilina Pali; HS, Hilina slump. Black line below K is the seismic (solid) and aseismic (dashed) position of the decollement from Got and Okubo [24]. Two thicker black lines with grey shaded area, family of geologically plausible dislocation solutions equivalently supported by inversion of GPS data. Colored circles indicate locations of microearthquakes from ±5 days around each slow earthquake event. Earthquakes are from the same source as Fig. 1. Coloring as in Fig. 1 (cyan, 20 Sept., 1998; orange, 9 Nov. 2000; yellow, 16 Dec. 2002; red, 26 Jan. 2005).

These different solutions have distinctly different implications for how strain is accommodated in the HS. Given that much of the inferred fault plane is offshore, that the GPS network geometry is seriously suboptimal for imaging deformation offshore, and the possibility of model specification errors (i.e. incomplete knowledge of SE physics), model preference cannot be assigned based on such small misfit differences.

Although not all SE source kinematics are well-constrained by the existing data, seismic moment, M_0 (defined as the product of shear modulus, slip magnitude, and slip area) can be constrained adequately for the January 2005 event (Fig. 4C). Using this as a reference we calculate M_0 (and equivalent moment magnitude, M_w) released in the other SEs (Fig. 4D). Consider two slow earthquake events, event j and event k, sharing the same focal mechanism. The seismic moment, M, of each event will be related to the observed surface displacements by:

$$M_j^2 = c \sum_i^{N_s} d_{ij} \cdot d_{ij} \quad (1)$$

where $d_{ij} \cdot d_{ij}$ represents the inner product of the surface displacements for the ith station during the jth (or kth) event; N_s is the number of stations (the same for each event); and c is a constant which is also the same for each event. The relationship between moments for each event is thus given by the ratio:

$$\frac{M_j^2}{M_k^2} = \frac{\sum_i^{N_s} d_{ij} \cdot d_{ij}}{\sum_i^{N_s} d_{ik} \cdot d_{ik}} \quad (2)$$

where the constant c has been cancelled. If a value for M_k is determined independently we can use (2) to calculate M_j. If no independent estimate for M_k is available, then M_j is a relative measure of moment.

M_w values for the September 1998, November 2000, December 2002 and January 2005 events are 5.6, 5.7, 5.5, and 5.8, respectively (Fig. 4D). Our $M_w \sim 5.7$ estimate for the November 2000 event is identical to the independent estimate of Cervelli et al. [35].

5. Relationship with seismicity

Microseismicity in the HS region is highly complex due to the various volcanic and gravitationally driven tectonic phenomena occurring in such close proximity [24]. Although none of the SEs are accompanied by conventional earthquakes greater than M 3.5, daily counts of microearthquakes show spikes at the times of the SEs, especially the January 2005 event (Fig. 2C). However, many spikes of activity are not associated with SEs. Although the mean value of the SE moments (3.97×10^{17} N m) is roughly equivalent to the cumulative earthquake moment release over the same time period (4.77×10^{17} N m), it does not appear that there is any obvious relationship between SE magnitude and earthquake seismicity in the entire HS volume (Fig. 4D). In early 2000, there was an earthquake rate increase that corresponds roughly with a moment rate increase, but these changes are not correlative with any SE signal.

The SEs, however, do appear to trigger a set of microearthquakes that occur in a confined ~NW–SE trending band terminating at the Hilina Pali (Fig. 1C–F). Plots of cumulative number for 80 days around each event demonstrate that the SEs are followed by a jump in seismicity in a region around the band (Fig. 6, box in Fig. 1B). In Fig. 5 we show a cross-section placing the HVO catalog locations (http://www.ncedc.org/) of these events in the context of the general structure of the HS and the family of good-fitting dislocation solutions for the SEs. The triggered earthquakes generally occur between ~5 and 10 km and with a N–S position below the Hilina Pali. Moreover, based on waveform cross-correlation relocation of thousands of Kīlauea events between 1988 and 1999, Got and Okubo [24] demonstrated that the same band of microearthquakes (Fig. 1B) occurs on a steeply south-dipping, subdecollement reverse fault plane (Fig. 5). Thus, it appears likely that the SEs regularly trigger seismicity near the decollement and that the triggered seismicity may occur on a well-defined fault plane. In order to verify this, future work will entail performing waveform cross-

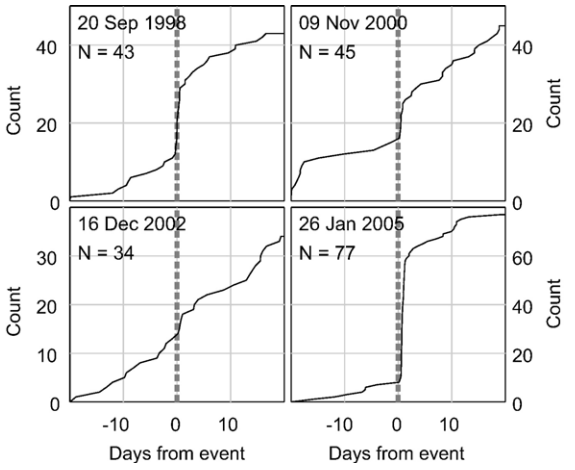

Fig. 6. Cumulative earthquake count from within the region defined by the yellow box in Fig. 1B for each slow earthquake. Data are from ±20 days of the onset of the event (grey dashed line).

correlation relocations for the entire catalog spanning all of the SE event times. If the events do, indeed, collapse to a well-defined plane then we will use this information to define the orientation of a 'receiver' fault in Coulomb stress change calculations that can be combined with the geodetic data in a joint inversion scheme. At the present time, however, the most we can say is that the catalog locations of the triggered events appear to favour the deeper dislocation solutions for the SEs.

6. Discussion

The detection of repeated, apparently periodic SEs at the HS means that the range of mechanical conditions permitting periodic SEs is likely not limited to the higher pressures and temperatures of subduction zones. Because the inversion results do not permit adequate resolution of SE source location and mechanism, however, we can at this time place only broad constraints on a possible mechanism for the SEs. One possibility is that overpressurized confined aquifers being recharged by surface water systems such as those found at ~3 km depth in the Hawai'i Scientific Drilling Project II borehole [39] could facilitate SE slip. This scenario presents a possible explanation for periodicity: the SE slip could rupture the confined aquifer and partially drain it. If the aquifer recharged at a constant rate, periodic slip could be facilitated each time some critical pressure threshold is exceeded.

SEs that occur in subduction zones are also associated with the newly identified phenomenon of seismic tremor [7,40]. Clearly it will be important to determine if tremor or a similar phenomenon accompanies the SEs in the HS. Even including the HS SEs, there is a very small number of natural examples of highly periodic fault slip behavior. Of these, the Parkfield, CA periodic behavior appears to have broken down with time [41] while Cascadia periodicity has persisted. Further measurements will be needed at the HS to document whether our observation of SE periodicity will hold true for future behavior. Additionally, in order to better constrain the geometry of the fault on which a future SE may occur, we will need concurrent deformation measurements on the submarine extension of the HS. The emerging field of seafloor geodesy [42,43] is the obvious approach, although the measurements we need must be made on a continuous basis.

Acknowledgements

We thank the Hawaiian Volcano Observatory (HVO-USGS), especially Asta Miklius, and Paul Segall of Stanford University for interchange of GPS data, and the National Park Service for their support in establishing our GPS network. Earthquake hypocenters were provided by the Northern California Earthquake Data Center (NCEDC) and HVOUSGS. Rainfall data was provided by the National Park Service. Special thanks to Fran Coloma and Ricky Herd for maintaining the GPS stations through the years, to David Okita for providing invaluable helicopter support, and to Paul Okubo, Jean-Luc Got, Juli Morgan, and Tomas Zapata for stimulating discussion. This work was supported by the Geophysics and Geochemistry programs of the US National Science Foundation. SOEST contribution # 6768.

References

[1] A.T. Linde, M.T. Gladwin, M.J.S. Johnston, R.L. Gwyther, R.G. Bilham, A slow earthquake sequence on the San Andreas Fault, Nature (Lond.) 383 (6595) (1996) 65–68.
[2] I.S. Sacks, S. Suyehiro, A.T. Linde, J.A. Snoke, Slow earthquakes and stress redistribution, Nature 275 (1978) 599–602.
[3] A.T. Linde, K. Suyehiro, S. Miura, I.S. Sacks, A. Takagi, Episodic aseismic earthquake precursors, Nature 334 (1988) 513–515.
[4] K. Heki, S.-I. Miyazaki, H. Tsuji, Silent fault slip following an interplate thrust earthquake at the Japan Trench, Nature 386 (6625) (1997) 595–598.
[5] H. Dragert, K. Wang, T.S. James, A silent slip event on the deeper Cascadia subduction interface, Science 292 (2001) 1525–1528.
[6] M.M. Miller, T.I. Melbourne, D.J. Johnson, W.Q. Sumner, Periodic slow earthquakes from the Cascadia Subduction Zone, Science 295 (2002) 2423.
[7] G. Rogers, H. Dragert, Episodic Tremor and slip on the Cascadia Subduction Zone: the chatter of silent slip, Science 300 (2003) 1942–1943.

[8] P. Cervelli, P. Segall, K. Johnson, M. Lisowski, A. Miklius, Sudden aseismic fault slip on the south flank of Kilauea volcano, Nature 415 (6875) (2002) 1014–1018.
[9] J. Freymueller, C. Zweck, H. Fletcher, S. Hreinsdottir, S.C. Cohen, M. Wyss, The great Alaska 'earthquake' of 1998–2001, EOS, Trans.-Am. Geophys. Union, vol. 82, 2001.
[10] V. Kostoglodov, S.K. Singh, A. Santiago, S.I. Franco, K.M. Larson, A.R. Lowry, R. Bilham, A large silent earthquake in the Guerrero seismic gap, Mexico, Geophys. Res. Lett. 30 (15) (2003) 1807, doi:10.1029/2003GL017219.
[11] K.M. Larson, A.R. Lowry, V. Kostoglodov, Crustal deformation measurements in Guerrero, Mexico, J. Geophys. Res. 92 (2004) 12,751–12,762.
[12] A.R. Lowry, K.M. Larson, V. Kostoglodov, R. Bilham, Transient fault slip in Guerrero, southern Mexico, Geophys. Res. Lett. 28 (2001) 3753–3756.
[13] K. Aki, M. Fehler, S. Das, Source mechanism of volcanic tremors: fluid driven crack models and their application to the 1963 Kilauea eruption, J. Volcanol. Geotherm. Res. (1977) 259–287.
[14] B. Julian, Seismological detection of slab metamorphism, Science 296 (2002) 1625–1626.
[15] H. Kao, S.-J. Shan, H. Dragert, G. Rogers, J.F. Cassidy, K. Ramachandran, A wide depth distribution of seismic tremors along the northern Cascadia margin, Nature 436 (2005) 841–844.
[16] S. Peacock, K. Wang, Seismic consequences of warm versus cool subduction metamorphism: examples from southwest and northeast Japan, Science 286 (1999) 937–939.
[17] S. Owen, et al., Rapid deformation of the south flank of Kilauea volcano, Hawaii, Science 267 (5202) (1995) 1328–1332.
[18] S. Owen, P. Segall, M. Lisowski, A. Miklius, R. Denlinger, M. Sako, Rapid deformation of Kilauea volcano: global positioning system measurements between 1990 and 1996, J. Geophys. Res. 105 (B8) (2000) 18,983–18,998.
[19] R.P. Denlinger, P. Okubo, Structure of the mobile south flank of Kilauea volcano, Hawaii, J. Geophys. Res. 100 (1995) 24,499–24,507.
[20] J.R. Smith, A. Malahoff, A.N. Shor, Submarine geology of the Hilina slump and morpho-structural evolution of Kilauea volcano, Hawaii, J. Volcanol. Geotherm. Res. 94 (1999) 59–88.
[21] J.K. Morgan, G.F. Moore, D.A. Clague, Slope failure and volcanic spreading along the submarine south flank of Kilauea volcano, Hawaii, J. Geophys. Res. 108 (B9) (2003) 2415, doi:10.1029/2003JB002411.
[22] J.G. Moore, W.R. Normark, R.T. Holcomb, Giant Hawaiian underwater landslides, Science 264 (5155) (1994) 46–47.
[23] S.N. Ward, Slip-sliding away, Nature 415 (2002) 973–974.
[24] J.-L. Got, P.G. Okubo, New insights into Kilauea's volcano dynamics brought by large-scale relative relocation of micro-earthquakes, J. Geophys. Res. 108 (B7) (2003), doi:10.1029/2002JB002060,2003.
[25] M. Ando, The Hawaii earthquake of November 29, 1975: low dip angle faulting due to forceful injection of magma, J. Geophys. Res. 94 (1979) 7616–7626.
[26] M. Wyss, A proposed source model for the Great Kau, Hawaii, earthquake of 1868, Bull. Seismol. Soc. Am. 78 (1988) 1450–1462.
[27] M. Nettles, G. Ekstrom, Long-period source characteristics of the 1975 Kalapana, Hawaii, earthquake, Bull. Seismol. Soc. Am. 94 (2004) 422–429.
[28] D.A. Swanson, W.A. Duffield, R.S. Fiske, Displacement of the south flank of Kilauea volcano: the result of forceful intrusion of magma into the rift zones, USGS Professional Paper, vol. 963, 1974.
[29] P.G. Okubo, H.M. Benz, B.A. Chouet, Imaging the crustal magma sources beneath Mauna Loa and Kilauea volcanoes, Hawaii, Geology 25 (20) (1997) 867–870.
[30] E.C. Cannon, R. Bürgmann, S.E. Owen, Shallow normal faulting and block rotation associated with the 1975 Kalapana earthquake, Kilauea volcano, Hawaii, Bull. Seismol. Soc. Am. 91 (6) (2001) 1553–1562.
[31] J.K. Morgan, G.F. Moore, D.J. Hills, S. Leslie, Overthrusting and sediment accretion along Kilauea's mobile south flank, Hawaii: evidence for volcanic spreading from marine seismic reflection data, Geology 28 (7) (2000) 667–670.
[32] R. King, Y. Bock, Documentation for the GAMIT GPS Analysis Software 2000, MIT and Scripps Inst. of Oceanogr., Cambridge, MA, 2000.
[33] D.J.I. Caccamise, M.A. Merrifield, M. Beivs, J. Foster, Y. Firing, M.S. Schenewerk, F.W. Taylor, D.T. Thomas, Sea level rise at Honolulu and Hilo, Hawaii: GPS estimates of differential land motion, Geophys. Res. Lett. 32 (2005).
[34] K. Heki, Seasonal modulation of interseismic strain buildup in Northeastern Japan driven by snow loads, Science 293 (89–92) (2001).
[35] P. Cervelli, C. Meertens, S. Owen, A. Miklius, M. Lisowski, P. Segall, F. Amelung, H. Garbeil, The 12 September 1999 Upper East Rift Zone dike intrusion at Kilauea volcano, Hawaii, J. Geophys. Res. B: Solid Earth 107 (7) (2002) 3-1–3-13.
[36] J. Dieterich, V. Cayol, P.G. Okubo, The use of earthquake rate changes as a stress meter at Kilauea volcano, Nature 408 (2000) 457–460.
[37] Y. Okada, Surface deformation due to shear and tensile faults in a halfspace, Bull. Seismol. Soc. Am. 75 (1985) 1135–1154.
[38] B. Brooks, L.N. Frazer, Importance reweighting reduces dependence on temperature in Gibbs samplers: an application to the coseismic geodetic inverse problem, Geophys. J. Int. 161 (1) (2005) 12–21.
[39] D.T. Thomas, Stratigraphy and hydrologic conditions in the HSDP II Borehole: implications for ocean island stability, Eos Trans. AGU, 86 (52), 2005, Fall Meet. Suppl.Abstract V21B-0606.
[40] K. Obara, Nonvolcanic deep tremor associated with subduction in southwest Japan, Science 296 (2002) 1679–1681.
[41] J. Murray, P. Segall, Testing time-predictable earthquake recurrence by direct measurement of strain accumulation and release, Nature 419 (2002) 287–291.
[42] K. Gagnon, C.D. Chadwell, E. Norabuena, Measuring the onset of locking in the Peru–Chile trench with GPS and acoustic measurements, Nature 434 (2005) 205–208.
[43] A. Sweeney, C.D. Chadwell, J.A. Hildebrand, F.N. Spiess, Centimeter-level positioning of seafloor acoustic transponders from a deeply-towed interrogator, Mar. Geol. 28 (2005) 39–70, doi:10.1080/01490410590884502.